ORAL/POSTER PRESENCE:0441

EVALUATION OF FRACTURE TOUGHNESS OF CERAMICS/METAL FUNCTIONALLY GRADED MATERIAL BY THREE-POINT-BENDING TEST

K. Tohgo [1], T. Suzuki [1], H. Araki [1] and H. Ishii [1]

[1] Department of Mechanical Engineering, Shizuoka University
3-5-1, Johoku, Hamamatsu 432-8561 Japan

ABSTRACT

This paper dealt with fracture toughness and fracture behavior of ceramics/metal functionally graded material (FGM). The used material was fabricated by powder metallurgy using partially stabilized zirconia (PSZ) and stainless steel (SUS 304). The material had a functionally graded surface layer (FGM layer) with a thickness of 1mm or 2mm on SUS 304 substrate. On the FGM layer, a volume fraction of PSZ varied from 100% at the surface to 10% at the interface between the FGM layer and substrate. In order to evaluate the fracture toughness of the FGM layer, three-point bending tests were carried out on a rectangular specimen with a very short crack in the ceramics surface. On the three-point bending test, unstable crack growth occurred from a short pre-crack to some amount of crack length, and then the crack grew stably to the interface between FGM layer and substrate with increasing the applied load. Finally, the crack was arrested at the SUS 304 substrate, and the specimen deformed plastically. From the relationship between the applied load and crack length during the stable crack growth in the FGM layer, fracture toughness was evaluated. The fracture toughness increases with an increase in a volume fraction of SUS 304. It is concluded that the three-point bending test of the rectangular specimen with a short pre-crack is useful to evaluate the distribution of fracture toughness in FGM layer.

KEYWARDS

Functionally graded materials, Fracture toughness, Three-point-bending test, Stable crack growth, Ceramics/metal composite

INTRODUCTION

Functionally graded materials (FGMs) in which material components or their contents vary in some direction have a large amount of potentiality as engineering materials because of their unique performance [1-6]. An FGM plate consisting of ceramics and metals, for example, can be designed to reduce the thermal stress and to maintain the heat resistance and ductility. In order to apply FGMs to the engineering structure, it is necessary to estimate the strength and fracture mechanism not only under thermal loading but also under external loading such as static and cyclic loads [2-6].

This paper dealt with the evaluation of fracture toughness and fracture behavior of ceramics/metal functionally graded material (FGM). A possibility of stable crack growth in a three-point-bending specimen was discussed based on the crack driving force and the crack growth resistance of FGM. Then, on a FGM consisting of partially stabilized zirconia (PSZ) and stainless steel (SUS 304), three-point- bending tests were carried out on a rectangular specimen with a very short crack in the ceramics surface, and the details of fracture process were observed by a CCD camera and a scanning electron microscope. From the relationship between the applied load and crack length during the stable crack growth in the FGM layer, the distribution of fracture toughness along the FGM layer was evaluated. The influence of material composition on the fracture toughness in FGM layer and the fracture behavior of the FGM were discussed.

STABILITY OF CRACK GROWTH IN THREE-POINT-BENDING SPECIMEN

In this section, the stability of crack growth in a three-point-bending specimen as shown in Fig. 1 is discussed. It is assumed that the three-point-bending test is conducted by displacement-control of a load-point, and the compliance of the testing machine is negligible because of very high stiffness. The energy release rate G is given by the well-known equation

$$G = \frac{1}{2} P^2 \frac{dC}{dA} = \frac{1}{2} \frac{\delta^2}{C^2} \frac{dC}{dA} \tag{1}$$

where, C=δ/P is compliance of the specimen. P, δ and A are load, load-point displacement and crack area, respectively. On the displacement-control test, the stable crack growth occurs under the condition of

$$G = G_{mat} \ , \qquad \left(\frac{\partial G}{\partial A} \right)_{\delta} \le \frac{dG_{mat}}{dA} \tag{2}$$

where, G and G_{mat} show the driving force and material resistance to crack growth, respectively. The stability of crack growth in the three-point-bending specimen is examined based on the above condition. The left hand term of Eq. (2-$_2$) is written as follows

$$\left(\frac{\partial G}{\partial A} \right)_{\delta} = \frac{1}{2} \frac{\delta^2}{C^2} \left\{ \frac{d^2 C}{dA^2} - \frac{2}{C} \left(\frac{dC}{dA} \right)^2 \right\} \tag{3}$$

For the three-point-bending specimen, the stress intensity factor is given as

$$K_I = F_I(a/W) \sigma_0 \sqrt{\pi a} \quad , \quad \sigma_0 = \frac{3PS}{2W^2 B} \tag{4}$$

where, $F_I(a/W)$is the correction factor, and a, W, B and S are crack length, width, thickness and span length of the specimen. By introducing the non-dimensional crack length and compliance

$$\alpha = \frac{a}{W} \ , \qquad C_0 = \frac{\delta / S}{\sigma_0 / E'} \tag{5}$$

the following relations are obtained

$$\frac{d}{dA} = \frac{1}{WB} \frac{d}{d\alpha} \ , \qquad \frac{d^2}{dA^2} = \frac{1}{W^2 B^2} \frac{d^2}{d\alpha^2} \ ,$$

$$C = \frac{3S^2}{2W^2 BE'} C_0 \tag{6}$$

By considering these relations, Eq. (3) becomes as follows.

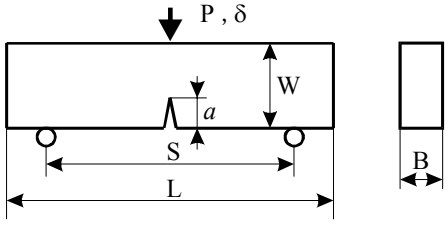

Figure 1: Three-point-bending specimen.

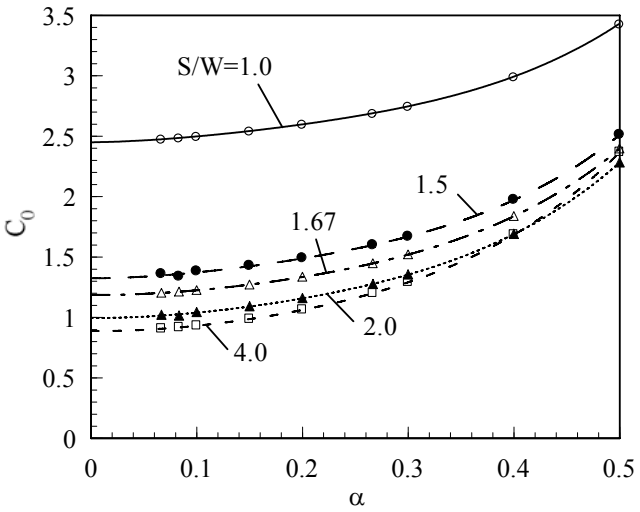

Figure 2: Nondimensional compliances of three-point-bending specimens.

$$\left(\frac{\partial G}{\partial \alpha}\right)_{\delta} = \frac{W}{3E'}\sigma_0{}^2\left\{\frac{d^2C_0}{d\alpha^2} - \frac{2}{C_0}\left(\frac{dC_0}{d\alpha}\right)^2\right\} \tag{7}$$

From the relation between the energy release rate and stress intensity factor

$$G = \frac{W}{3E'}\sigma_0{}^2\frac{dC_0}{d\alpha} = \frac{K_I{}^2}{E'} = \frac{W}{E'}\sigma_0{}^2\pi\{F_I(\alpha)\}^2\alpha \tag{8}$$

the following relation is obtained

$$\frac{dC_0}{d\alpha} = 3\pi\{F_I(\alpha)\}^2\alpha \tag{9}$$

By substituting Eq. (9) into Eq. (7), and considering Eqs. (2-$_1$) and (8), the following non-dimensional stability factor is obtained.

$$\frac{1}{G_{mat}}\left(\frac{\partial G}{\partial \alpha}\right)_{\delta} = \frac{1}{\{F_I(\alpha)\}^2\alpha}\left\{2F_I(\alpha)\frac{dF_I(\alpha)}{d\alpha}\alpha + \{F_I(\alpha)\}^2 - \frac{6\pi}{C_0}\{F_I(\alpha)\}^4\alpha^2\right\} \tag{10}$$

In the present investigation, Eq. (10) is evaluated based on the results of finite element analyses of the three-point-bending specimens with different ratio of span to width. Figures 2, 3 and 4 show the results of the non-dimensional compliance, correction factor of stress intensity and stability factor as functions of crack length for the three-point-bending specimens. From the condition of stable crack growth, the high value of the stability factor means that the unstable crack growth is easy to occur. As shown in Fig. 4, the stability factor in the region of short crack length is insensitive to the span to width ratio and it is higher for the shorter crack. When we consider the ceramics/metal functionally graded materials (FGM), the fracture toughness increases from ceramics surface to inside with an increase in a metal volume fraction. For example, the following linear relation is postulated for the distribution of fracture toughness.

$$K_{Imat} = K_{cer} + K\alpha \tag{11}$$

Since G_{mat} is obtained as

$$G_{mat} = \frac{K_{Imat}{}^2}{E'} = \frac{1}{E'}\left(K_{cer}{}^2 + 2K_{cer}K\alpha + K^2\alpha^2\right) \tag{12}$$

The gradient of material resistance is obtained as follows

$$\frac{1}{G_{mat}}\left(\frac{\partial G_{mat}}{\partial \alpha}\right) = \frac{2k + 2k^2\alpha}{1 + 2k\alpha + k^2\alpha^2} \quad , \qquad \frac{K}{K_{cer}} = k \tag{13}$$

In Fig. 4, the above equation is plotted for several k-values. This figure provides us with the information of stability of crack growth in the given specimen (S/W) and material (k). For example, if we conduct the

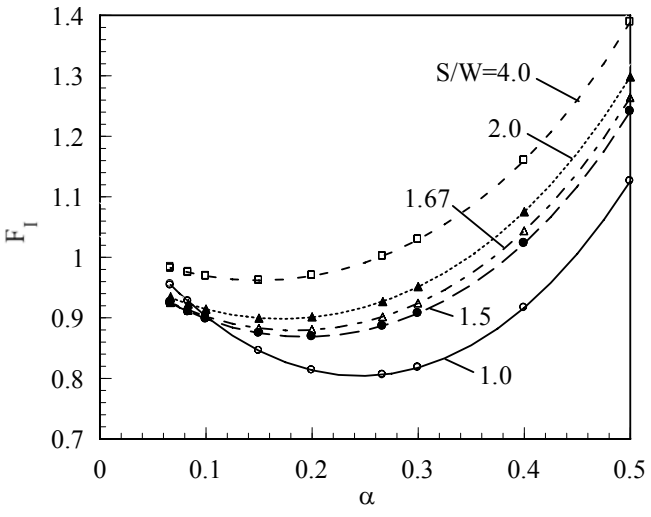

Figure 3: Correction factors of three-point-bending specimens.

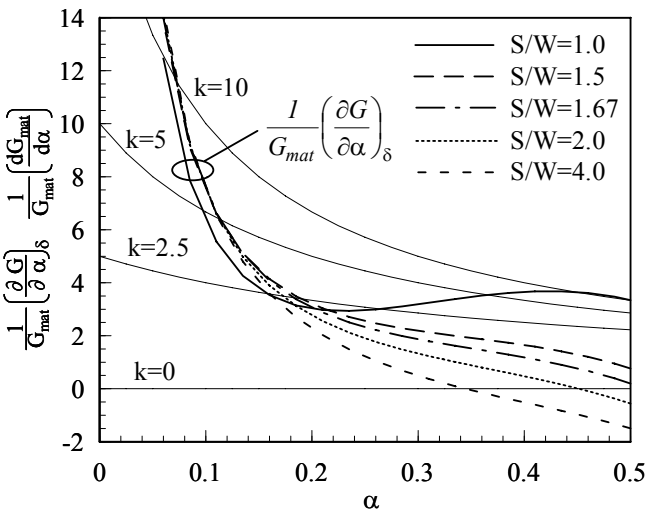

Figure 4: Stability of crack growth in three-point-bending specimens.

experiment for the material as shown by k=5 with the specimen with S/W=4, the crack growth becomes unstable to α=0.12 and then becomes stable for longer crack than α=0.12. Although the stable crack growth is obtained for longer crack than α=0.34 on the monolithic ceramics (k=0), the crack growth becomes stable in the wide region from shorter crack length on the FGM with high gradient of material resistance. Figure 4 is useful in the determination of the specimen size to obtain the stable crack growth in the given FGM.

MATERIALS AND EXPERIMENTAL PROCEDURE

The used material was fabricated by powder metallurgy using partially stabilized zirconia (ZrO_2-3molY_2O_3, PSZ) and stainless steel (SUS 304). The material has a functionally graded surface layer (FGM layer) on SUS 304 substrate. Figure 5 shows the configuration of three-point-bending specimen and the details of the FGM layer. The FGM layer consists of multi-layers in which a volume fraction of PSZ varies stepwise from 100% at the surface to 10% at the interface between the FGM layer and substrate. Two kinds of FGMs were fabricated, in which thickness of the FGM layers were designed to be about 1mm and 2mm; hereafter they are referred as FGM-1 and FGM-2, respectively. The SUS 304 particles were dispersed in the PSZ matrix in the layers from 100% PSZ to 40% PSZ, and on the contrary, the PSZ particles were dispersed in the SUS 304 matrix in the layers from 20% PSZ to 10% PSZ. The width of the specimen was 6mm, and the span length was changed in 24mm (S/W=4.0), 12mm (S/W=2.0) and 10mm (S/W=1.67). A series of median cracks by Vickers indentation were introduced as a starter-crack on the ceramics surface of the three-point-bending specimen. The depth of the median cracks was about 300μm.

Three-point-bending tests were conducted with 0.05mm/min crosshead speed at the room temperature and air. During test, the relation between load (P) and load-point-displacement (δ) was recorded, and the crack length and fracture process were observed on a side surface of the specimen by a CCD camera. The critical stress intensity factor was calculated from relationship between the load and crack length during stable crack growth. On the fractured specimen, the details of fracture surfaces were examined by a scanning electron microscope (SEM).

RESULTS AND DISCUSSION

Figure 6 shows an example of load-displacement relation obtained by three-point-bending test of FGM-2 and Fig. 7 exhibits the observation of a side surface of the specimen by CCD camera. As shown in Fig. 7, the stable crack growth is obtained in the FGM layer. The crack length measured on the video by a CCD

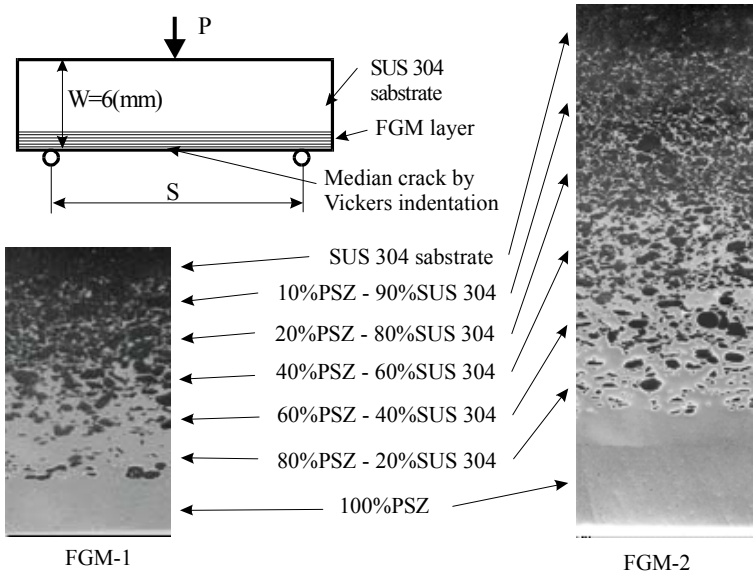

Figure 5: Specimen configuration and details of the FGM layer.

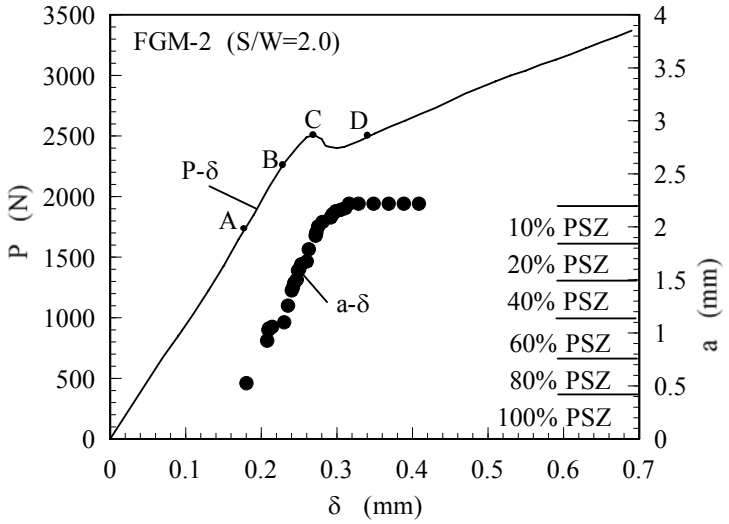

Figure 6: Load and crack length as functions of load-point displacement.

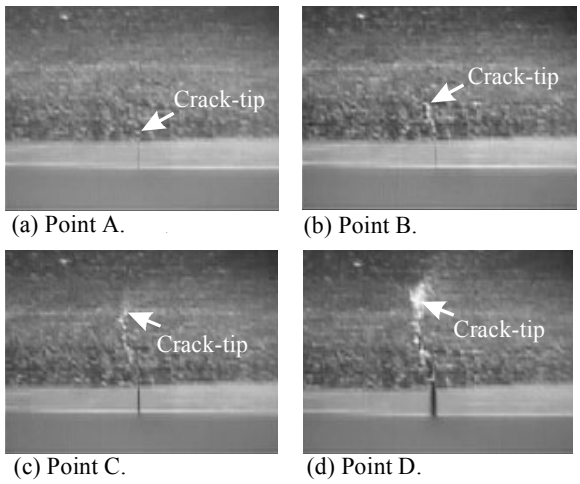

Figure 7: Stable crack growth in FGM layer.

camera is also plotted in Fig. 6. When the applied load reaches the critical value for the initial indentation crack at the point A in Fig. 6, the unstable crack growth occurs from the initial crack to 80% PSZ layer. However, any signal such as load drop is not observed on the load-displacement relation. Then, a crack grows stably to the interface between FGM layer and SUS 304 substrate with increasing the applied load. The load-displacement relation shows the slight nonlinearity before the growing crack reaches the 20% PSZ layer (Point C). At this point, the plastic zone spread out from the crack tip into the SUS304 substrate, and the applied load once drops then increases with increasing the displacement. The crack grows gradually into the plastically deformed 10% PSZ layer and finally is arrested at the SUS 304 substrate (Point D). This feature is almost the same as that observed in the FGM-1.

From the relationship between the applied load and crack length during the stable crack growth, the critical stress intensity factor K_{IC} is calculated for each specimen. Figures 8 and 9 show the critical stress intensity factor as a function of crack length in FGM-1 and FGM-2, respectively. These figures exhibit the distributions of fracture toughness through the FGM layers since the crack length means the distance from the ceramics surface. The fracture toughness linearly increases with an increase in the distance from ceramics surface through the FGM layer. Although the slight difference in the distribution among the specimens is observed even in the same kind of FGM, it may be attributed to the difference in the thickness of FGM layer, the distribution of the PSZ content, the residual stress created in the fabrication, the span-to-width ratio of three-point-bending specimen and so on. In order to clarify the difference, further investigations are necessary.

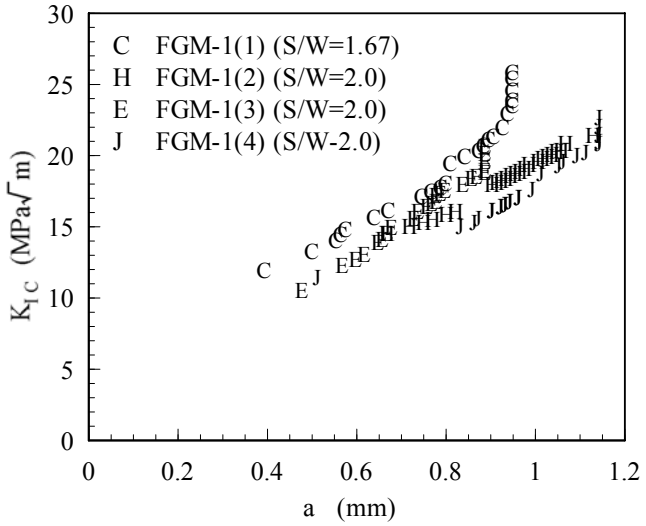

Figure 8: Distributions of fracture toughness in FGM-1 specimens.

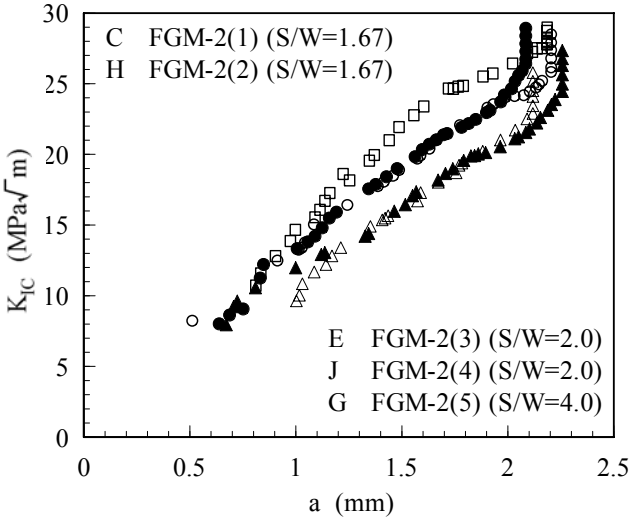

Figure 9: Distributions of fracture toughness in FGM-2 specimens.

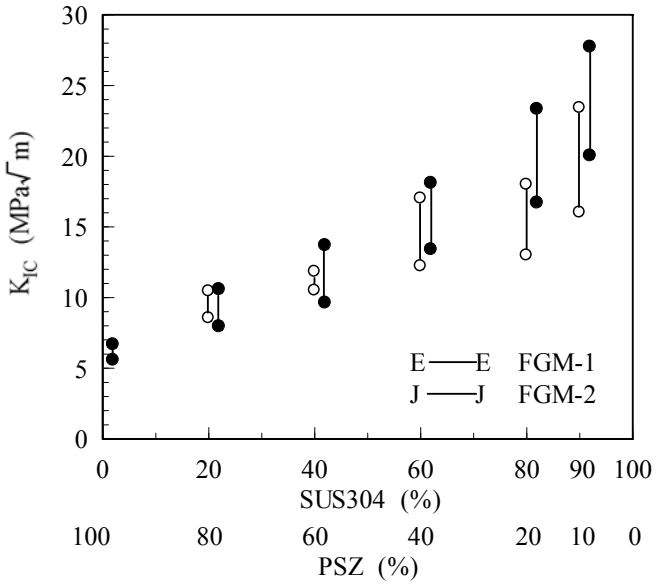

Figure 10: Fracture toughness as a function of material composition in FGM layer.

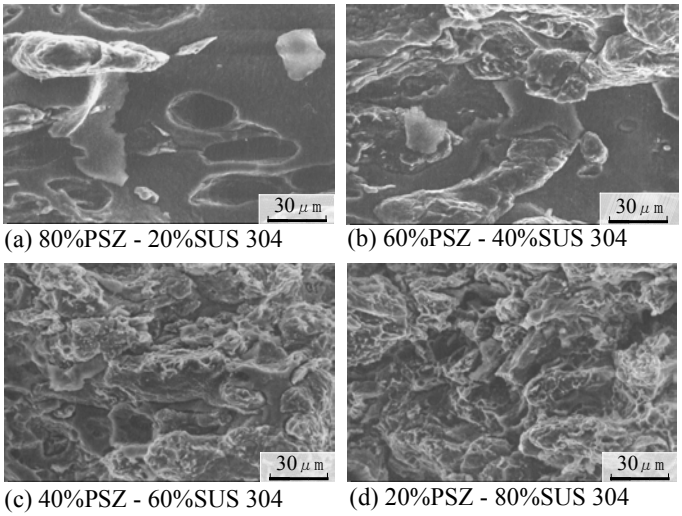

(a) 80%PSZ - 20%SUS 304 (b) 60%PSZ - 40%SUS 304

(c) 40%PSZ - 60%SUS 304 (d) 20%PSZ - 80%SUS 304

Figure 11: Micrographs of fracture surfaces of FGM layer.

In order to obtain the relationship between the fracture toughness and composition of PSZ and SUS 304 in the FGM layer, the experimental results in Figs. 8 and 9 are rearranged as in Fig. 10. The fracture toughness of the PSZ ceramics (FGM-2) and 80%PSZ layer (FGM-1) is evaluated from the unstable crack growth of the initial indentation crack with 300μm in length. The fracture toughness in FGM layer in both materials is well described by the unique relation, namely it linearly increases with an increase in SUS304 content up to 90%. It is concluded from Fig. 10 that the distribution of fracture toughness through the FGM layer is given as a function of the composition of PSZ and SUS 304. The fracture toughness in the FGM layer is at most 30MPa m at 90% PSZ layer, and is very low compared with the fracture toughness of 100% SUS 304. This might be caused by the intrinsic property of the FGM that the fracture toughness abruptly drops between 100% SUS 304 and 90% SUS 304 in addition to that the influence of the plastic deformation is not considered in the evaluation of the fracture toughness.

Micrographs of fracture surface of the FGM are shown in Fig. 11. In the layers with high content of PSZ as shown in Figs. 11(a) and (b), the debonded SUS 304 particles and their traces are observed in the brittle fracture surface of the PSZ matrix. This means that the interfacial strength between the SUS 304 particles and PSZ matrix is relatively low. On the other hand, the metal rich layers exhibit the brittle fracture surface of PSZ phase in the ductile fracture surface of the SUS 304 matrix as shown in Figs. 11(c) and (d). With increasing the content of SUS 304, the area of ductile fracture surface with dimple-pattern increases. This well corresponds to the distribution of the fracture toughness in FGM layer as shown in Fig. 10.

REFERENCES

1. For example, (1991). Functionally Gradient Materials, Kogyo Chosakai Publishing (in Japanese).
2. Finot, M., Suresh, S., Bull, C., Giannakopoulos, A.E., Olsson M. and Sampath, S. (1994). Proc.3rd Int. Symp. Struct. Funct. Grad. Mater., 229.
3. Kawasaki, A. and Watanabe, R. (1994). Proc. 3rd Int. Symp. Struct. Funct. Grad. Mater., 397.
4. Blumm, M., Dollmeler, K. and Ilschner, B. (1994). Proc. 3rd Int. Symp. Struct. Funct. Grad. Mater., 315.
5. Tohgo, K., Sakaguchi, M. and Ishii, H. (1996). JSME Int. J., Ser. A. 39, 479.
6. Tohgo, K. and Hadano, A. (1999). Proc. Exper. Comput. Mech., 81.